1-Butyl-3-methylimidazolium Tosylate Ionic Liquid: Heat Capacity, Thermal Stability, and Phase Equilibrium of Its Binary Mixtures with Water and Caprolactam

Aliaksei A. Strechan, Yauheni U. Paulechka, Andrey G. Kabo, Andrey V. Blokhin, and Gennady J. Kabo*

Chemistry Faculty, Research Institute for Physical Chemical Problems, Belarusian State University, Leningradskaya 14, Minsk, 220030

Heat capacity for 1-butyl-3-methylimidazolium tosylate [C_4mim][Tos] in the temperature range (5 to 370) K has been measured by adiabatic calorimetry. Temperatures and enthalpies of its phase transitions have been determined. Thermodynamic functions have been calculated for crystalline and liquid states. The thermal stability of [C_4mim][Tos] has been determined by scanning calorimetry. Mutual solubility in binary mixtures of [C_4mim]-[Tos] with water and caprolactam has been investigated, and the activity coefficients have been calculated. Heat capacities for three mixtures of [C_4mim][Tos] with water have been measured by adiabatic calorimetry. On the basis of the calorimetric and SLE measurements for ([C_4mim][Tos] + water) samples the heat capacity anomalies have been interpreted.

Introduction

Organic salts with T_{fus} < 373 K, ionic liquids (ILs), have a great potential for their technical and technological use due to a unique combination of physical and chemical properties: high conductivity, great thermal, chemical, and electrochemical stability, low vapor pressure, catalytic activity, etc.[1−3]

For justification of conditions for synthesis and technological application of ILs, it is extremely important to know their thermodynamic properties in a wide interval of temperatures. Application of ILs will essentially depend on their thermal stability, the ability to form eutectics and solutions with freezing temperatures much lower than those for parent ILs. There are a few works which contain the results of high-quality thermodynamic investigations of ILs by adiabatic calorimetry.[4−9] As stated,[5−7] the fractional melting technique used in adiabatic calorimetry is among the best methods for determination of total impurity content.

In this work, we report the results of a thermodynamic study of 1-butyl-3-methylimidazolium tosylate [C_4mim][Tos]. They include heat capacities and enthalpies of phase transitions in the temperature range of (5 to 470) K, thermal stability, heat capacities, and mutual solubility in binary mixtures of [C_4mim]-[Tos] with water and phase equilibria of [C_4mim][Tos] with caprolactam. These properties will allow us to evaluate the ability of [C_4mim][Tos] to be used as an extragent and desiccant in caprolactam production.

Experimental

Sample Preparation. A commercial sample of [C_4mim][Tos] was kindly provided by Prof. A. Heintz from the University of Rostock (Germany). The [C_4mim][Tos] sample was purified by vacuum pumping during 30 h at T rising from (323 to 353) K. This period was long enough to get the mass of the sample constant within the weighing threshold of ± 5·10^{-5} g.

* Corresponding author. Telephone: +375-17-2003916. Fax: +375-17-2003916. E-mail address: kabo@bsu.by.

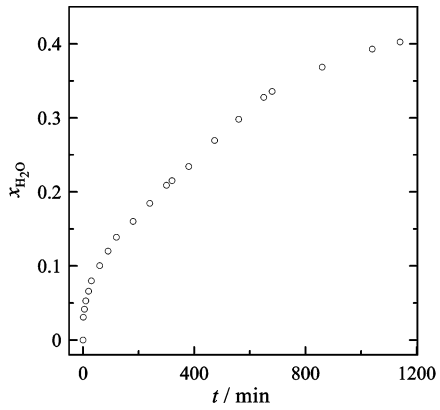

Figure 1. Hygroscopicity of [C_4mim][Tos] at T = 293 K.

To be sure that crystalline [C_4mim][Tos] would be stable in the conditions of the measurements, its hygroscopicity and thermal stability were determined. Hygroscopicity was measured at T = (293 ± 1) K and air humidity of 55 %. Powder-like [C_4mim][Tos] (m = 0.2225 g) was loaded into an aluminum cup and exposed to air. The changes in the sample mass were periodically registered. As seen from the results presented in Figure 1, [C_4mim][Tos] being a hydrophilic IL absorbs ≈ 10 % of water during the first hour. Therefore, it can be used as a desiccant.

According to DSC, this compound remains stable to 470 K (Figure 2). The only endothermic peak in the range of (320 to 347) K corresponds to fusion of the sample.

The mole fraction purity of the sample was determined by the fractional melting technique. The experimental data (Table 1) were fitted with the use of the equation[10]

$$\ln\left(\frac{\nu}{f}+1\right)=\frac{\Delta_{fus}H^\circ}{RT_{fus}^{\ 2}}\cdot(T_{fus}-T)+\frac{\Delta_{fus}H^\circ}{RT_{fus}^{\ 2}}\cdot\left(\frac{1}{T_{fus}}-\frac{\Delta C_p(T_{fus})}{2\Delta_{fus}H^\circ}\right)\cdot(T_{fus}-T)^2 \quad (1)$$

10.1021/je700152c CCC: $37.00
Published on Web 08/07/2007

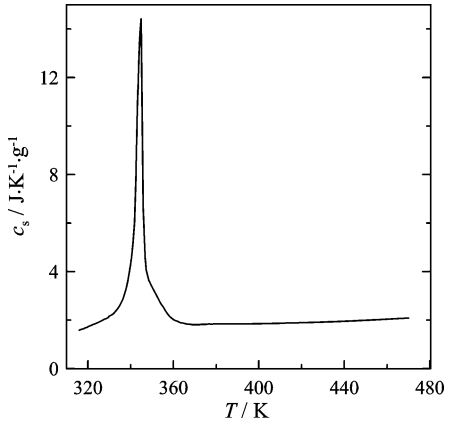

Figure 2. Experimental heat capacities c_s for [C_4mim][Tos] measured by differential scanning calorimetry.

Table 1. Results of Fractional Melting *f* for [C_4mim][Tos] (Sample No. 1)[a]

T/K	f
Crystal I′	
Series 4	
332.709	0.3076
333.846	0.3526
334.855	0.4051
335.738	0.4650
336.505	0.5317
337.161	0.6049
337.720	0.6838
338.201	0.7674
338.629	0.8541
	T_{fus} = (342.48 ± 0.07) K
Crystal I	
Series 5	
333.937	0.2583
335.410	0.2905
336.731	0.3308
337.863	0.3815
338.801	0.4422
339.574	0.5122
340.159	0.5919
340.712	0.6737
341.161	0.7612
341.522	0.8531
	T_{fus} = (343.63 ± 0.20) K
	x = (0.960 ± 0.002)
Series 6	
334.091	0.2484
335.520	0.2799
336.799	0.3193
337.912	0.3677
338.856	0.4251
339.650	0.4906
340.261	0.5655
340.841	0.6448
341.282	0.7293
341.593	0.8208
	T_{fus} = (343.97 ± 0.11) K
	x = (0.960 ± 0.001)

[a] f is the melting fraction at temperature T; T_{fus} is the triple point of the compound; and x is the mole fraction purity of the sample.

where υ is the amount of impurities in a sample, mole per mole of the main substance; f is the equilibrium melt fraction at temperature T; $\Delta_{fus}H°$ is the enthalpy of fusion for a pure compound; and ΔC_p is the heat capacity change at fusion of a pure compound. The mole purity fraction of the sample was found to be (0.960 ± 0.002). If one supposes water to be the main impurity, the mass fraction purity is 0.998.

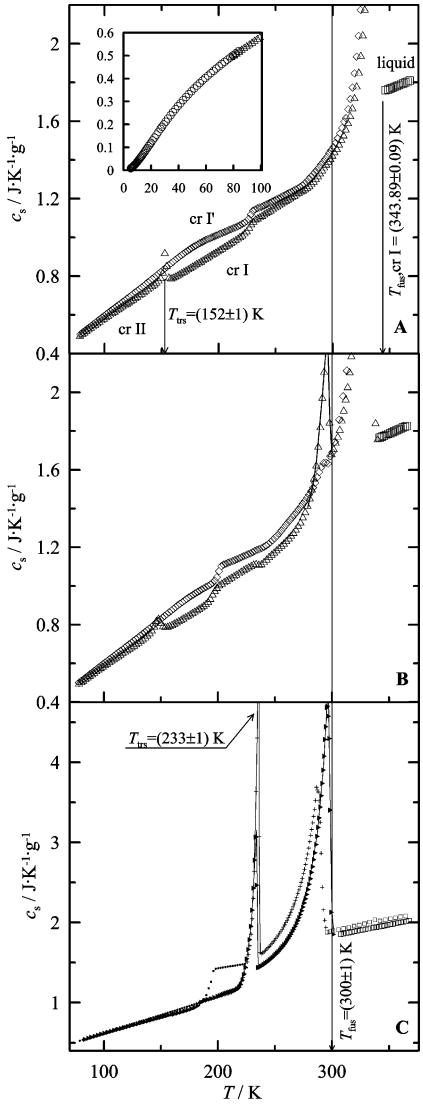

Figure 3. Experimental heat capacities c_s for [C_4mim][Tos]: ◇, experimental points for cr I′; △, for cr I and cr II; ○, for cr I; ●, for glass; ▲ and +, for crystal (unknown type); □, for liquid. Water content, x(H_2O): A, 0.04; B, 0.17; C, ▲, 0.63; +, 0.70.

Adiabatic Calorimetry. Heat capacities in the condensed state in a range of temperatures of (5 to 370) K and phase transition enthalpies were measured in a TAU-10 vacuum adiabatic calorimeter. The calorimeter and the procedure of measurements were described in ref 7. The temperature was measured with an iron/rhodium resistance thermometer (R_0 = 50 Ω) calibrated on ITS-90 by VNIIFTRI (Moscow). The sample was loaded into a container in a drybox to prevent contamination with moisture from air. A temperature step of the measurements outside the phase-transition intervals did not exceed 2 K.

The uncertainty of heat capacity measurements was assumed to be ± 0.4 % in the temperature range of (20 to 370) K, 1 % at (10 to 20) K, and < 2 % below 10 K.[7]

Differential Scanning Calorimetry. Heat capacities of [C_4mim][Tos] in a range of temperatures of (315 to 470) K were measured with a one-cup scanning calorimeter.[11] The calorimeter was calibrated with reference corundum (VNIIM, St.-Petersburg, Russia). The following equation was used for the reference corundum

$$C_p/\mathrm{J{\cdot}K^{-1}{\cdot}g^{-1}} = (-267.77 + 4.9399(T/\mathrm{K}) - 0.0047954(T/\mathrm{K})^2)/1000 \quad (2)$$

Table 2. Experimental Heat Capacities at Saturation Pressure c_s for [C_4mim][Tos]

Series 1

T/K	c_s^a/J·g^{-1}·K^{-1}	T/K	c_s^a/J·g^{-1}·K^{-1}	T/K	c_s^a/J·g^{-1}·K^{-1}	T/K	c_s^a/J·g^{-1}·K^{-1}	T/K	c_s^a/J·g^{-1}·K^{-1}	T/K	c_s^a/J·g^{-1}·K^{-1}
Crystal											
300.21	1.419	311.99	1.545	323.37	1.825	331.77	2.658	337.59	6.112	340.52	15.33
302.10	1.435	313.94	1.576	325.17	1.912	333.19	3.028	338.36	7.432	340.89	17.10
304.10	1.453	315.87	1.609	326.92	2.024	334.49	3.525	339.03	8.938	341.25	15.94
306.09	1.473	317.78	1.651	328.62	2.175	335.65	4.179	339.61	10.83	341.66	10.53
308.07	1.494	319.67	1.698	330.24	2.384	336.69	5.000	340.10	12.95	342.74	2.089
310.04	1.519	321.53	1.755								
Liquid											
344.54	1.757	353.97	1.779	363.42	1.801	346.43	1.760	353.97	1.779	361.53	1.797
346.43	1.760	355.86	1.783	365.30	1.805	348.31	1.764	355.86	1.783	363.42	1.801
348.31	1.764	357.74	1.788	367.19	1.810	350.20	1.770	357.74	1.788	365.30	1.805
350.20	1.770	359.64	1.792	344.54	1.757	352.08	1.775	359.64	1.792	367.19	1.810
352.08	1.775	361.53	1.797								

Series 2

T/K	c_s^a/J·g^{-1}·K^{-1}	T/K	c_s^a/J·g^{-1}·K^{-1}	T/K	c_s^a/J·g^{-1}·K^{-1}	T/K	c_s^a/J·g^{-1}·K^{-1}	T/K	c_s^a/J·g^{-1}·K^{-1}	T/K	c_s^a/J·g^{-1}·K^{-1}
Crystal I′											
78.68	0.4999	119.62	0.6835	159.92	0.8740	199.61	1.013	241.45	1.169	282.53	1.323
80.67	0.5087	121.45	0.6915	161.74	0.8825	201.47	1.019	243.33	1.174	284.36	1.336
82.53	0.5166	123.28	0.6997	163.55	0.8909	203.39	1.024	245.21	1.179	286.18	1.348
84.39	0.5256	125.12	0.7080	165.36	0.8992	205.31	1.028	247.08	1.185	288.00	1.361
86.26	0.5343	126.95	0.7164	167.18	0.9073	207.23	1.033	248.96	1.190	289.81	1.375
88.14	0.5425	128.79	0.7246	168.99	0.9153	209.16	1.038	250.83	1.196	291.62	1.389
90.02	0.5512	130.63	0.7332	170.80	0.9231	211.08	1.042	252.70	1.201	293.42	1.403
91.92	0.5598	132.46	0.7418	172.60	0.9307	213.00	1.047	254.58	1.207	295.21	1.417
93.82	0.5687	134.30	0.7501	174.41	0.9379	214.92	1.051	256.45	1.213	296.99	1.434
95.72	0.5772	136.14	0.7588	176.21	0.9448	216.84	1.057	258.32	1.219	298.77	1.450
97.64	0.5856	137.98	0.7679	178.02	0.9515	218.76	1.062	260.20	1.225	300.54	1.467
99.55	0.5943	139.81	0.7765	179.82	0.9577	220.68	1.069	262.07	1.230	302.41	1.488
101.42	0.6025	141.65	0.7852	181.62	0.9638	222.60	1.075	263.94	1.235	304.39	1.511
103.22	0.6108	143.48	0.7939	183.43	0.9699	224.51	1.085	265.82	1.242	306.36	1.536
105.03	0.6187	145.31	0.8030	185.23	0.9755	226.41	1.096	267.69	1.248	308.32	1.565
106.84	0.6267	147.15	0.8116	187.02	0.9809	228.30	1.118	269.56	1.253	310.26	1.598
108.66	0.6349	148.98	0.8206	188.82	0.9861	230.18	1.137	271.43	1.260	311.76	1.616
110.48	0.6429	150.80	0.8295	190.62	0.9910	232.06	1.144	273.30	1.268	313.67	1.662
112.31	0.6505	152.63	0.8385	192.42	0.9958	233.94	1.150	275.16	1.276	315.56	1.714
114.13	0.6588	154.46	0.8474	194.22	1.001	235.82	1.154	277.01	1.287	317.42	1.774
115.96	0.6669	156.28	0.8564	196.01	1.005	237.70	1.158	278.86	1.300	319.26	1.847
117.79	0.6748	158.10	0.8653	197.81	1.009	239.58	1.163	280.70	1.313	321.06	1.933

Series 3

T/K	c_s^a/J·g^{-1}·K^{-1}	T/K	c_s^a/J·g^{-1}·K^{-1}	T/K	c_s^a/J·g^{-1}·K^{-1}	T/K	c_s^a/J·g^{-1}·K^{-1}	T/K	c_s^a/J·g^{-1}·K^{-1}	T/K	c_s^a/J·g^{-1}·K^{-1}
Crystal II											
78.41	0.4962	91.63	0.5519	104.79	0.6052	117.62	0.6545	130.57	0.7046	143.59	0.7605
80.40	0.5045	93.54	0.5599	106.61	0.6123	119.46	0.6614	132.43	0.7120	145.44	0.7698
82.25	0.5119	95.45	0.5678	108.44	0.6193	121.30	0.6685	134.29	0.7195	147.30	0.7802
84.11	0.5203	97.37	0.5757	110.27	0.6263	123.16	0.6758	136.15	0.7275	149.15	0.7930
85.98	0.5284	99.29	0.5833	112.10	0.6331	125.01	0.6826	138.01	0.7357	150.98	0.8213
87.86	0.5363	101.16	0.5907	113.94	0.6405	126.86	0.6900	139.87	0.7437	152.77	0.9224
89.74	0.5439	102.98	0.5978	115.78	0.6478	128.72	0.6970	141.73	0.7518		
Crystal I											
154.55	0.8561	188.19	0.8916	222.77	1.024	256.99	1.185	288.90	1.334	321.05	1.783
156.40	0.7953	190.05	0.8982	224.72	1.035	258.88	1.192	290.72	1.349	322.89	1.854
158.27	0.7914	191.90	0.9048	226.65	1.053	260.77	1.199	292.53	1.364	324.69	1.941
160.14	0.7957	193.75	0.9116	228.56	1.070	262.65	1.206	294.33	1.379	326.45	2.047
162.02	0.8010	195.60	0.9183	230.47	1.083	264.53	1.212	296.13	1.394	328.17	2.180
163.89	0.8069	197.45	0.9244	232.37	1.095	266.42	1.219	297.92	1.408	329.82	2.346
165.76	0.8130	199.30	0.9318	234.27	1.101	268.31	1.226	299.71	1.426	331.67	2.681
167.64	0.8195	201.21	0.9389	236.17	1.108	270.19	1.232	301.60	1.443	333.72	3.138
169.51	0.8260	203.18	0.9458	238.07	1.115	272.08	1.239	303.60	1.460	335.54	3.839
171.39	0.8324	205.15	0.9531	239.97	1.122	273.97	1.245	305.59	1.483	337.10	4.830
173.26	0.8390	207.12	0.9603	241.87	1.129	275.87	1.252	307.57	1.507	338.39	6.066
175.13	0.8455	209.08	0.9676	243.76	1.135	277.76	1.260	309.54	1.530	339.46	7.536
177.01	0.8522	211.04	0.9749	245.66	1.142	279.64	1.268	311.49	1.561	340.31	9.585
178.87	0.8587	213.00	0.9819	247.55	1.150	281.51	1.278	313.44	1.594	340.98	11.81
180.74	0.8654	214.96	0.9895	249.44	1.157	283.38	1.291	315.37	1.630	341.41	15.40
182.60	0.8719	216.91	0.9973	251.33	1.164	285.23	1.305	317.29	1.670	341.94	11.46
184.47	0.8783	218.87	1.005	253.22	1.171	287.07	1.318	319.18	1.722	343.81	1.772
186.33	0.8850	220.82	1.013	255.11	1.178						
Liquid											
346.46	1.761	350.60	1.769	354.36	1.777	358.12	1.787	361.88	1.796	365.62	1.804
348.72	1.764	352.48	1.773	356.25	1.782	360.00	1.791	363.75	1.800	367.50	1.809

Table 2 (Continued)

Series 4

T/K	c_s^a/J·g^{-1}·K^{-1}	T/K	c_s^a/J·g^{-1}·K^{-1}	T/K	c_s^a/J·g^{-1}·K^{-1}	T/K	c_s^a/J·g^{-1}·K^{-1}	T/K	c_s^a/J·g^{-1}·K^{-1}	T/K	c_s^a/J·g^{-1}·K^{-1}
Crystal I′											
311.76	1.616	319.26	1.847	326.19	2.345	332.06	3.661	336.12	7.158	338.42	13.74
313.67	1.662	321.06	1.933	327.77	2.562	333.27	4.265	336.84	8.586	338.86	13.25
315.56	1.714	322.82	2.040	329.28	2.834	334.34	5.033	337.45	10.32	339.51	5.836
317.42	1.774	324.53	2.175	330.69	3.192	335.29	6.000	337.97	12.16	340.93	1.749
Liquid											
342.82	1.749	344.72	1.755	346.61	1.759	348.49	1.763				

Series 5

T/K	c_s^a/J·g^{-1}·K^{-1}	T/K	c_s^a/J·g^{-1}·K^{-1}	T/K	c_s^a/J·g^{-1}·K^{-1}	T/K	c_s^a/J·g^{-1}·K^{-1}	T/K	c_s^a/J·g^{-1}·K^{-1}	T/K	c_s^a/J·g^{-1}·K^{-1}
Crystal II											
78.30	0.4956	91.54	0.5517	104.71	0.6052	117.56	0.6547	130.54	0.7048	143.56	0.7621
80.29	0.5039	93.45	0.5596	106.53	0.6122	119.41	0.6617	132.40	0.7120	145.41	0.7746
82.14	0.5119	95.36	0.5675	108.37	0.6192	121.26	0.6684	134.26	0.7199	147.26	0.7931
84.01	0.5198	97.28	0.5755	110.20	0.6263	123.11	0.6756	136.12	0.7276	149.09	0.8270
85.88	0.5276	99.21	0.5832	112.03	0.6333	124.97	0.6828	137.98	0.7356	150.89	0.8780
87.76	0.5357	101.08	0.5905	113.87	0.6402	126.82	0.6900	139.84	0.7438	152.68	0.8713
89.65	0.5437	102.89	0.5978	115.71	0.6475	128.68	0.6973	141.70	0.7522		
Crystal I											
154.51	0.8010	188.19	0.8916	222.83	1.022	257.06	1.183	290.68	1.350	324.63	1.903
156.37	0.7872	190.05	0.8981	224.77	1.037	258.94	1.189	292.49	1.365	326.41	2.002
158.25	0.7896	191.91	0.9049	226.70	1.052	260.82	1.197	294.29	1.376	328.13	2.128
160.13	0.7949	193.77	0.9117	228.61	1.069	262.71	1.203	296.09	1.390	329.79	2.290
162.00	0.8008	195.62	0.9183	230.52	1.081	264.59	1.210	297.87	1.405	331.45	2.574
163.88	0.8069	197.47	0.9250	232.43	1.092	266.47	1.216	299.66	1.420	333.13	2.855
165.76	0.8131	199.32	0.9316	234.33	1.101	268.36	1.223	301.54	1.439	334.68	3.251
167.63	0.8195	201.24	0.9390	236.24	1.105	270.25	1.230	303.54	1.458	336.08	3.782
169.51	0.8261	203.21	0.9467	238.14	1.112	272.14	1.235	305.52	1.478	337.32	4.603
171.38	0.8327	205.18	0.9536	240.04	1.119	274.03	1.242	307.50	1.501	338.37	5.739
173.25	0.8390	207.15	0.9604	241.94	1.126	275.92	1.250	309.47	1.526	339.23	7.211
175.13	0.8454	209.12	0.9679	243.83	1.133	277.80	1.258	311.42	1.555	339.93	9.023
177.00	0.8521	211.09	0.9751	245.73	1.140	279.67	1.267	313.37	1.587	340.47	10.75
178.87	0.8585	213.05	0.9823	247.62	1.147	281.53	1.279	315.30	1.622	340.97	13.43
180.74	0.8650	215.01	0.9896	249.51	1.155	283.38	1.291	317.22	1.659	341.38	15.83
182.60	0.8719	216.97	0.9974	251.40	1.161	285.22	1.306	319.11	1.705	341.62	37.41
184.47	0.8783	218.93	1.005	253.29	1.169	287.05	1.320	320.98	1.758	342.27	4.129
186.33	0.8850	220.88	1.013	255.17	1.175	288.87	1.336	322.82	1.823		
Liquid											
343.97	1.752	346.06	1.755	348.14	1.759						

Series 6

T/K	c_s^a/J·g^{-1}·K^{-1}	T/K	c_s^a/J·g^{-1}·K^{-1}	T/K	c_s^a/J·g^{-1}·K^{-1}	T/K	c_s^a/J·g^{-1}·K^{-1}	T/K	c_s^a/J·g^{-1}·K^{-1}	T/K	c_s^a/J·g^{-1}·K^{-1}
Crystal II											
80.63	0.5052	93.92	0.5614	107.00	0.6137	119.87	0.6632	130.97	0.7063	142.13	0.7532
82.63	0.5134	95.83	0.5692	108.83	0.6208	121.71	0.6702	132.83	0.7137	143.98	0.7621
84.49	0.5215	97.75	0.5769	110.67	0.6278	123.56	0.6773	134.69	0.7215	145.83	0.7719
86.36	0.5296	99.67	0.5845	112.50	0.6351	125.41	0.6844	136.55	0.7292	147.68	0.7840
88.24	0.5375	101.54	0.5921	114.34	0.6420	127.27	0.6915	138.41	0.7369	149.52	0.8046
90.12	0.5457	103.36	0.5994	116.18	0.6492	129.12	0.6989	140.27	0.7447	151.34	0.8609
92.02	0.5536	105.18	0.6065	118.02	0.6561						
Crystal I											
153.11	0.9269	188.51	0.8926	223.07	1.023	257.23	1.186	290.87	1.353	324.85	1.864
154.91	0.8124	190.37	0.8995	225.01	1.036	259.11	1.193	292.67	1.366	326.64	1.957
156.77	0.7887	192.22	0.9063	226.94	1.057	261.00	1.200	294.47	1.377	328.38	2.076
158.64	0.7909	194.07	0.9131	228.85	1.075	262.87	1.207	296.27	1.392	330.07	2.227
160.51	0.7960	195.92	0.9194	230.75	1.085	264.75	1.213	298.05	1.407	331.71	2.504
162.38	0.8020	197.77	0.9261	232.65	1.096	266.63	1.219	299.83	1.424	333.31	2.732
164.25	0.8080	199.61	0.9324	234.55	1.104	268.52	1.227	301.72	1.442	334.81	3.094
166.12	0.8145	201.52	0.9400	236.45	1.109	270.40	1.233	303.71	1.462	336.18	3.592
168.00	0.8209	203.49	0.9470	238.35	1.116	272.29	1.239	305.69	1.482	337.39	4.289
169.87	0.8273	205.46	0.9544	240.25	1.124	274.19	1.245	307.67	1.505	338.42	5.269
171.74	0.8338	207.42	0.9614	242.14	1.130	276.08	1.251	309.64	1.531	339.29	6.481
173.61	0.8402	209.38	0.9684	244.04	1.137	277.97	1.259	311.59	1.560	340.02	7.908
175.48	0.8469	211.34	0.9761	245.93	1.144	279.85	1.268	313.53	1.590	340.59	9.407
177.35	0.8535	213.31	0.9834	247.82	1.151	281.71	1.279	315.46	1.621	341.10	12.05
179.21	0.8600	215.27	0.9911	249.71	1.158	283.57	1.293	317.39	1.650	341.50	15.20
181.08	0.8663	217.22	0.9984	251.59	1.165	285.41	1.307	319.29	1.689	341.63	98.63
182.94	0.8730	219.18	1.007	253.47	1.172	287.24	1.322	321.17	1.734	341.99	6.464
184.80	0.8795	221.13	1.014	255.35	1.179	289.06	1.339	323.03	1.791	343.34	1.841
186.66	0.8861										
Liquid											
345.34	1.754	348.77	1.764	352.50	1.773	356.24	1.782	359.97	1.791	361.84	1.796
347.35	1.758	350.64	1.769	354.37	1.778	358.11	1.787				

Table 2 (Continued)

Series 7

T/K	c_s^a/J·g^{-1}·K^{-1}	T/K	c_s^a/J·g^{-1}·K^{-1}	T/K	c_s^a/J·g^{-1}·K^{-1}	T/K	c_s^a/J·g^{-1}·K^{-1}	T/K	c_s^a/J·g^{-1}·K^{-1}	T/K	c_s^a/J·g^{-1}·K^{-1}
5.19	0.00909	9.06	0.03167	15.52	0.08281	27.91	0.1901	45.37	0.3195	65.48	0.4336
5.39	0.01009	9.46	0.03446	16.38	0.09057	29.13	0.2003	47.37	0.3325	67.50	0.4439
5.69	0.01153	9.86	0.03729	17.25	0.09804	30.61	0.2125	49.38	0.3451	69.52	0.4537
5.99	0.01302	10.37	0.04114	18.11	0.1053	32.24	0.2259	51.39	0.3572	71.55	0.4634
6.33	0.01478	10.99	0.04576	18.98	0.1126	34.04	0.2399	53.40	0.3691	73.58	0.4732
6.71	0.01683	11.62	0.05074	19.85	0.1201	35.85	0.2538	55.41	0.3805	75.61	0.4827
7.10	0.01905	12.24	0.05552	21.02	0.1302	37.65	0.2667	57.43	0.3916	77.64	0.4918
7.49	0.02132	12.87	0.06059	22.47	0.1429	39.46	0.2797	59.46	0.4026	79.68	0.5011
7.88	0.02375	13.50	0.06572	23.94	0.1560	41.36	0.2927	61.48	0.4130	81.72	0.5101
8.27	0.02627	14.13	0.07089	25.40	0.1687	43.36	0.3062	63.50	0.4236	83.76	0.5195
8.67	0.02893	14.77	0.07631	26.86	0.1813						

[a] Average heat capacity at the mean temperature of an experiment.

The deviations of the experimental heat capacities from the values calculated from eq 2 were < 0.5 %

The [C$_4$mim][Tos] sample (m = 112.9 mg) was loaded into an aluminum cup. The internal space of the calorimeter was filled with argon at P = 6 kPa. The temperature of the cup was measured with a iron/constantan differential thermocouple. A platinum resistance thermometer (100 Ω) was used as a temperature sensor. The average scanning rate was 1.0 K·min^{-1}.

SLE Measurements. Mutual solubilities of [C$_4$mim][Tos] with water and caprolactam were determined by a visual method. A mixture of known composition was heated very slowly in a water thermostat. To reach SLE (solid−liquid equilibria), the heating rate did not exceed 1.0 K·h^{-1}, in the very closeness to the saturation temperature. The saturation temperature was assumed to be the temperature at which the last crystal disappeared. The temperature was measured with thermometers with an uncertainty of ± 0.25 K in the range of (260 to 290) K and ± 0.05 K in the range of (290 to 340) K. The experiment was repeated at least twice for each composition. The saturation temperatures were reproducible within 0.1 K.

Results and Discussion

Heat Capacity of Liquid. Experimental heat capacities for liquid [C$_4$mim][Tos] from DSC and from adiabatic calorimetry are presented in Figures 2 and 3, respectively. The data from the two methods were jointly treated by the least-squares method, and the following equations were obtained for the temperature ranges of (348 to 385) K

$$C_{p,\mathrm{m}}(\mathrm{liq})/\mathrm{J{\cdot}K^{-1}{\cdot}mol^{-1}} = (-1.762 + 2.362(T/\mathrm{K}) - 2.257{\cdot}10^{-3}(T/\mathrm{K})^2) \quad (3)$$

and (385 to 470) K

$$C_{p,\mathrm{m}}(\mathrm{liq})/\mathrm{J{\cdot}K^{-1}{\cdot}mol^{-1}} = (1.775{\cdot}10^{3} - 6.434(T/\mathrm{K}) + 8.586{\cdot}10^{-3}(T/\mathrm{K})^2) \quad (4)$$

Crystal Phases. The experimental c_s values for the [C$_4$mim][Tos] sample in the temperature range of (5 to 370) K are presented in Table 2 and Figure 3A. The history of calorimetric measurements and the procedures for preparation of phases are shown in Table 3 and Figure 4.

[C$_4$mim][Tos] was found to form two crystalline modifications depending on the crystallization procedure. The modification with higher T_{fus} is designated as cr I, and that with lower T_{fus} is designated as cr I′ (Table 3).

(a) Crystal I′. It was found in series 1 that the [C$_4$mim][Tos] sample had a pre-melting range of (280 to 345) K. Liquid [C$_4$mim][Tos] at cooling from 370 K with an initial rate of (0.02 to 0.03) K·s^{-1} was cooled to T = 312 K where spontaneous crystallization occurred. In 5 min, the sample reached T = 318 K, the maximum temperature of the crystallization process. After holding at this temperature for 3 h, the heat evolution due to the crystallization ceased. Then, the sample was heated to T = 337 K in the heat capacity measurement mode and annealed at the latter temperature. As a result, cr I′ was formed (Table 3, Figure 4).

The sample was cooled to 77 K, and then its heat capacity was measured (series 2). The spontaneous exothermic cr I′ → cr I transition began above T = 320 K. If cr I′ was cooled from 337 K to only 310 K, in consequent experiments it melted without transition into cr I (series 4). The results from series 2 and 4 were combined to obtain the whole heat capacity curve for cr I′. The triple-point temperature T_{fus} for cr I′ was determined to be T_{fus} = (342.48 ± 0.08) K by the fractional melting technique (Table 1). In these experiments (series 4), the equilibration time was 400 s.

(b) Crystal I. On the basis of the results from series 2, the following procedure was applied to obtain cr I. cr I′ after series 2 cooled to 77 K was heated to 337 K and annealed at this temperature for 20 h. This resulted in formation of cr I (Table 3, Figure 4).

The triple-point temperature T_{fus} = (343.89 ± 0.09) K was determined from the fractional melting experiments (Table 1). Because cr I was stable in the pre-melting region, the equilibration time was increased to 2000 s.

There is a sigmoid anomaly in the heat capacity curves for both the crystals at T > 215 K (Figure 3A). Such a behavior may be related to the formation of glass composed of an IL and impurity. This agrees with the results described below for sample no. 4. A kink in the C_p vs T curve in the range of (270 to 280) K (Figure 3A) is accompanied by abnormally high-temperature drifts of the calorimeter and long equilibration time. Crystallization of the glassy phase seems to be a possible cause of this kink.

(c) Crystal II. A solid−solid transition (cr II → cr I) is observed in the range of temperatures from (130 to 163) K with a maximum at T = (152 ± 1) K (Figure 3A). The enthalpy change $\Delta_{\mathrm{crII}}^{\mathrm{crI}}H^\circ$ = (194 ± 2) J·mol^{-1} was calculated by numeric integration (Table 4). The following baselines were chosen for the crystals:

$$C_{p,\mathrm{m}}(\mathrm{cr\ II})/\mathrm{J{\cdot}K^{-1}{\cdot}mol^{-1}} = (73.37 + 1.080(T/\mathrm{K})) \quad (5)$$

$$C_{p,\mathrm{m}}(\mathrm{cr\ I})/\mathrm{J{\cdot}K^{-1}{\cdot}mol^{-1}} = (62.18 + 1.199(T/\mathrm{K})) \quad (6)$$

They were obtained from the experimental heat capacities in the temperature ranges (101 to 133) K for cr II and (162 to 188) K for cr I.

Table 3. Description of the Series of Calorimetric Experiments for [C_4mim][Tos]

	preparation procedure			heat capacity measurements	
series	formation	annealing, heating	cooling	phases	T/K
			Sample No. 1 (m_s = 0.6944 g)		
1				Cr I′	300 to 342
2	cooling of liquid from 350 K, onset of crystallization at 312 K	3 h at 318 K, heating up to 335 K in the heat capacity measurement mode, then annealing for 2 h at 335 K	to 310 K at a rate of 0.003 K·s^{-1}, then to 77 K at (0.02 to 0.01) K·s^{-1}	Cr I′ (above 320 K, positive temperature drifts of calorimeter (conversion into cr I))	78 to 321
3	after series 2	19 h at 337 K	to 310 K at a rate of 0.003 K·s^{-1}, then to 77 K at (0.02 to 0.01) K·s^{-1}	Cr I, II, liquid	78 to T_{fus} T_{fus} to 367
4	cooling of liquid from 370 K, onset of crystallization at 311 K	3 h at 317 K, heating up to 336 K in the heat capacity measurement mode, then annealing for 15 h at 336 K	to 310 K at a rate of 0.003 K·s^{-1}	Cr I′, liquid	311 to T_{fus} T_{fus} to 348
5	like in series 3			Cr I, II, liquid	78 to T_{fus} T_{fus} to 348
6	like in series 3			Cr I, II, liquid	80 to T_{fus} T_{fus} to 361
7	like in series 3		from 300 K to 77 K (nitrogen bath) from 77 K to 5 K (helium bath)	Cr II	5 to 84
			Sample No. 2 (0.7007 g, 0.17 H_2O)		
8	cooling of liquid from 370 K, onset of crystallization at 304 K	6 h at 304 K to 305 K	to 290 K at 0.003 K·s^{-1}, to 77 K at (0.02 to 0.01) K·s^{-1}	Cr I′$_{H_2O,x_2=0.17}$ (above 310 K, positive temperature drifts of calorimeter (conversion into crystal I$_{H_2O,x_2=0.17}$))	79 to 311
9	after series 8		to 290 K at 0.003 K·s^{-1}, to 77 K at (0.02 to 0.01) K·s^{-1}	Cr I$_{H_2O,x_2=0.17}$	77 to 365
			Sample No. 3 (0.5419 g, 0.63 H_2O)		
10	cooling of liquid from 350 K		to 77 K at (0.02 to 0.01) K·s^{-1}	glass, supercooled liquid	77 to T_g T_g to 230
11	cooling of liquid from 230 K	heat capacity measurements from 180 K, then after onset of crystallization at 235 K, annealing during 17 h; cooling to 180 K, heat capacity measurement from 180 K, above 200 K − positive temperature drifts of calorimeter − annealing for 21 h	to 180 K at 0.003 K·s^{-1}, to 162 K at (0.02 to 0.01) K·s^{-1}	crystal, liquid	162 to T_{fus} T_{fus} to 370
			Sample No. 4 (0.5418 g, 0.70 H_2O)		
12	cooling of liquid from 350 K	heat capacity measurements from 180 K, then after onset of crystallization at 249 K, annealing during 17 h; cooling to 180 K, heat capacity measurement from 180 K, above 200 K − positive temperature drifts of calorimeter − annealing for 18 h	to 180 K at 0.003 K·s^{-1}, to 134 K at (0.02 to 0.01) K·s^{-1}	crystal, liquid	134 to T_{fus} T_{fus} to 370

Fusion. The fusion enthalpies were determined for every crystal phase (Table 4) using the equation

$$\Delta_{fus}H^\circ_m = Q - \int_{T_{start}}^{T_{fus}} C_{p,m}(\text{cr})dT - \int_{T_{fus}}^{T_{end}} C_{p,m}(\text{liq})dT \quad (7)$$

where Q is the energy required to heat 1 mol of substance from T_{start} to T_{end}. Initial T_{start} and final T_{end} temperatures lay outside the fusion range. Heat capacities of the crystals were described by the following equations obtained from the experimental heat capacities in the temperature ranges of (239 to 277) K for cr I and (237 to 273) K for cr I′

$$C_{p,m}(\text{cr I})/\text{J·K}^{-1}\text{·mol}^{-1} = (-4.846 + 1.763(T/\text{K}) - 1.227\cdot10^{-3}(T/\text{K})^2) \quad (8)$$

$$C_{p,m}(\text{cr I′})/\text{J·K}^{-1}\text{·mol}^{-1} = (3.068\cdot10^2 - 4.039(T/\text{K}) + 2.634\cdot10^{-3}(T/\text{K})^2) \quad (9)$$

The $\Delta_{fus}H^\circ_m$ (cr I) = (22.8 ± 0.5) kJ·mol^{-1} measured by DSC is in good agreement with the results from adiabatic calorimetry.

Thermodynamic Properties. Thermodynamic properties were calculated for cr I, the more stable crystalline modification of [C_4mim][Tos]. The smoothed values of thermodynamic functions for [C_4mim][Tos] in the crystalline and liquid states are presented in Table 5. Smoothing of experimental heat capacities was carried out with the use of polynomials.

A sum of Debye (D) and Einstein (E) contributions each having 3 degrees of freedom was used to extrapolate heat capacity of the substance down to 0 K. Because in the low-temperature range (T < 10 K) one may neglect the difference between $C_{s,m}$ and $C_{v,m}$

$$C_{s,m} \approx C_{v,m} = 3RD(\langle\Theta_D\rangle/T) + 3RE(\langle\Theta_E\rangle/T) \quad (10)$$

where Θ_D and Θ_E are the Debye and Einstein characteristic

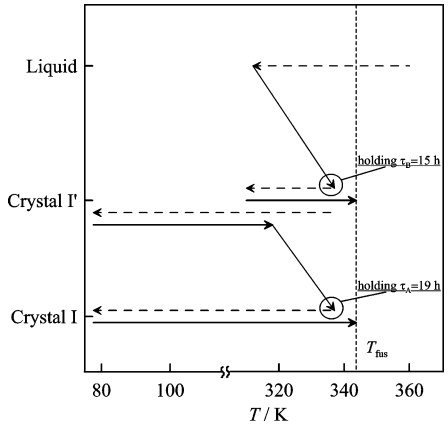

Figure 4. Evolution of calorimetric measurements when obtaining the crystalline phases of [C_4mim][Tos]: dotted line, cooling; thin solid line, phase transition; bold solid line, heat capacity measurements.

temperatures. They were obtained by the least-squares fitting of the experimental heat capacities in a range of temperatures of (5.19 to 9.06) K: $\Theta_D = 45.0$ K and $\Theta_E = 72.1$ K. The deviation of the experimental heat capacities from those calculated from eq 10 is < 1.5 % and does not exceed the experimental uncertainties in this interval.

The standard thermodynamic functions of cr I [C_4mim][Tos] at $T = 298.15$ K are equal to

$$C^\circ_{p,m} = (412.7 \pm 1.7)\ \text{J·K}^{-1}\text{·mol}^{-1}$$
$$\Delta_0^T S^\circ_m = (486.5 \pm 1.9)\ \text{J·K}^{-1}\text{·mol}^{-1}$$
$$\Delta_0^T H^\circ_m/T = (230.4 \pm 0.9)\ \text{J·K}^{-1}\text{·mol}^{-1}$$
$$\Phi^\circ_m = (256.0 \pm 1.0)\ \text{J·K}^{-1}\text{·mol}^{-1}$$

([C4mim][Tos] + Water) and ([C4mim][Tos]+ Caprolactam) SLE. The experimental SLE temperatures for ([C_4mim][Tos] + water) binaries are presented in Table 6 and Figure 5. The SLE diagram was obtained in a range of concentrations of x([C_4mim][Tos]) = (0.4 to 1.0). At the lower mole fractions of ILs, the solution did not crystallize under conditions of the experiments. The activity coefficients γ_i of [C_4mim][Tos] (Table 6) were calculated with the use of the following equation

$$\gamma_i = \frac{1}{x_{sat}} \exp\left[-\frac{\Delta_{fus}H^\circ_m(T_{sat})}{R}\left(\frac{1}{T_{sat}} - \frac{1}{T_{fus}}\right) - \frac{\Delta C_p}{R}\left(\ln\frac{T_{fus}}{T_{sat}} - \frac{T_{fus}}{T_{sat}} + 1\right)\right] \quad (11)$$

where x_{sat} is the mole fraction of a solute in the saturated solution; $\Delta_{fus}H^\circ_m(T_{sat})$ is the enthalpy of fusion of the solute at the saturation temperature T_{sat}; T_{fus} is the melting temperature of the pure solute; and ΔC_p is the heat capacity change at the saturation temperature.

The ideal SLE curves were calculated using the equation

$$\left(\frac{\partial \ln x_{sat}}{\partial T}\right) = \frac{\Delta_{fus}H^\circ_m}{RT^2_{fus}} \quad (12)$$

The significant deviation of the activity coefficients from unity is observed at low water content. A peritectic point was found in the SLE diagram at x([C_4mim][Tos]) = 54 % and T_{pp} = (300 ± 1) K (Figure 5).

The experimental mole compositions of the ([C_4mim][Tos] + caprolactam) binaries and their melting temperatures are presented in Table 6 and Figure 6. The activity coefficients of [C_4mim][Tos] calculated from eq 11 are given in Table 6. They indicate that solution of caprolactam with an IL behaves closely to the ideal one. The eutectic point is observed at x([C_4mim][Tos]) = 45.1 % and (T_e = 308.2 ± 0.5) K

Table 4. Determination of the Molar Enthalpies of Transition and Fusion for [C_4mim][Tos]

series number	T_{start} / K	T_{end} / K	Q / J·mol^{-1}	$\Delta_{fus}H^\circ_m$ / J·mol^{-1}
		cr II − cr I		
3	131.56	162.92	7606	194
5	131.52	162.91	7611	194
6	131.95	163.29	7610	195
				(194 ± 2)
		cr I′ − liq		
2 + 4	273.30	343.51	50443	(19915 ± 86)[a]
		cr I − liq		
3	277.60	347.46	51605	21567[b]
5	277.60	347.12	51441	21605[a]
6	277.60	345.78	50620	21547[a]
				(21573 ± 64)[c]

[a] From the fractional melting experiments. [b] From the simple heat capacity experiments. [c] Average value.

Effect of Water on the [C4mim][Tos] Heat Capacity. (a) Heat Capacity of Sample No. 2: [C4mim][Tos] (1)/H2O (2), x1 = 0.83. A portion of 6.3 mg of water was added to the initial sample of IL (sample No.2, Table 3) to clarify the nature of anomalies in the heat capacity curve of [C_4mim][Tos].

The heat capacity of sample no. 2 was measured in a range of temperatures of (77 to 370) K (Table 1S, Supporting Information). The procedures for preparation of the phases were similar to those described for the initial sample (Table 3).

The solution of [C_4mim][Tos] and water was supercooled to $T = 304$ K at which spontaneous crystallization began. The annealing at (304 to 305) K for 6 h and cooling to 77 K were followed by the calorimetric experiments in a range of temperatures of (77 to 311) K (series 8). Above 310 K, cr $I'_{(H_2O,x_2=0.17)}$ was converted into cr $I_{(H_2O,x_2=0.17)}$. The only essential change in the $C_p(T)$ curve compared to the initial sample was a shift of the sigmoid anomaly from (220 to 240) K for cr I′ to (190 to 210) K for cr $I'_{(H_2O,x_2=0.17)}$ (Figure 3B). Unusually high-temperature drifts and the equilibration times were observed after passing the anomaly range both for cr I′ and cr $I'_{(H_2O,x_2=0.17)}$.

Cooling the sample after series 8 to 77 K was followed by the heat capacity measurements (series 9, cr$I_{(H_2O,x_2=0.17)}$). Again, the sigmoid anomaly was shifted (Figure 3B). A peak appeared in the heat capacity curve at $T = (300 \pm 1)$ K with the enthalpy of $\Delta_{fus}H^\circ = 7.5$ J·g^{-1}. This peak coincides with a peritectic point in the SLE diagram and corresponds to the fusion of the ([C_4mim][Tos] + H_2O) crystal hydrate. This transition was hardly detectable in the initial sample due to the lower water content (Figure 3A). The fusion of [C_4mim][Tos] occurred at $T_{fus} = (339 \pm 1)$ K.

(b) Heat Capacity of Sample No. 3: [C4mim][Tos] (1)/H2O (2), x1 = 0.37. The next addition of water to the sample (sample no. 3, Table 3) leads to essential changes in thermal behavior of the ([C_4mim][Tos] + H_2O) system. The liquid mixture was supercooled and formed glass. The heat capacity of the glass was measured in series 10. The glass-transition range was (183 to 200) K. The heat capacity of the supercooled liquid was measured in a range of (200 to 230) K.

The experimental heat capacity of sample no. 3 is presented in Figure 3C and Table 2S (Supporting Information). As for sample no. 2, there was a shift of the sigmoid anomaly to lower

Table 5. Thermodynamic Properties for cr I [C$_4$mim][Tos] (R = 8.31447 J·K^{-1}·mol^{-1})

T/K	$C^\circ_{p,m}/R$	$\Delta_0^T H^\circ_m/RT$	$\Delta_0^T S^\circ_m/R$	$-\Delta_0^T G^\circ_m/RT$
		Crystal II		
0	0	0	0	0
5	0.306	0.0157	0.1051	0.0894
10	1.432	0.4198	0.6319	0.2121
15	2.924	1.000	1.487	0.4875
20	4.531	1.683	2.550	0.8670
25	6.166	2.416	3.736	1.321
30	7.753	3.174	5.002	1.828
35	9.228	3.935	6.310	2.374
40	10.58	4.683	7.632	2.949
45	11.84	5.409	8.951	3.543
50	13.02	6.112	10.26	4.149
60	15.14	7.443	12.83	5.383
70	17.03	8.680	15.30	6.624
80	18.76	9.833	17.69	7.859
90	20.36	10.91	19.99	9.080
100	21.88	11.94	22.22	10.28
105	22.62	12.43	23.30	10.88
110	23.34	12.91	24.37	11.47
120	24.78	13.84	26.47	12.63
130	26.22	14.73	28.51	13.77
140	27.66	15.60	30.50	14.90
150	29.09	16.46	32.46	16.00
152.77	29.49	16.69	32.99	16.31
		Crystal I		
152.77	28.67	16.84	33.15	16.31
160	29.61	17.40	34.50	17.10
170	30.91	18.15	36.33	18.18
180	32.21	18.90	38.13	19.23
190	33.53	19.63	39.91	20.28
200	34.87	20.36	41.66	21.30
210	36.26	21.09	43.40	22.31
220	37.68	21.81	45.12	23.31
230	40.34	22.55	46.85	24.30
240	41.89	23.33	48.60	25.27
250	43.28	24.10	50.34	26.24
260	44.64	24.86	52.06	27.20
270	45.98	25.62	53.77	28.15
280	47.30	26.37	55.47	29.10
290	48.60	27.11	57.15	30.04
298.15	49.64	27.72	58.51	30.80
300	49.87	27.85	58.82	30.97
310	51.12	28.58	60.47	31.89
320	52.35	29.31	62.12	32.81
330	53.56	30.02	63.75	33.72
340	54.74	30.73	65.36	34.63
343.89	55.17	30.99	65.95	34.96
		Liquid		
343.67	65.35	38.54	73.50	34.96
350	65.96	39.03	74.70	35.67
360	66.87	39.79	76.57	36.78
370	67.73	40.53	78.41	37.88
380	68.53	41.26	80.23	38.97
390	68.78	41.96	82.02	40.05
400	69.20	42.64	83.76	41.12
410	69.83	43.30	85.48	42.18
420	70.66	43.94	87.17	43.23
430	71.70	44.57	88.85	44.28
440	72.94	45.20	90.51	45.31
450	74.39	45.83	92.16	46.33
460	76.05	46.47	93.82	47.35
470	77.92	47.12	95.47	48.35

temperatures without the increase in the heat capacity jump. A similar sigmoid anomaly was observed in the heat capacity curve of [C$_4$mim][Br].[5] It was related with the presence of water in a sample. However, in the ([C$_4$mim][Br] + H_2O) system, the magnitude of the anomaly increased with the increase of water content, but its temperature range was not shifted.

A peak with the maximum temperature T = (233 ± 1) K and enthalpy $\Delta_{trs}H^\circ$ = 11.6 J·g^{-1} was found. There are at least two possibilities for interpretation of this transition. The first one is the appearance of some kind of disorder in the lattice. The second one is the formation of a eutectic at T = 233 K. The rough extrapolation of the data on solubility (Figure 5) leads

Table 6. Experimental Activity Coefficients γ_i for [C$_4$mim][Tos] Binaries

x_1	T_{sat}/K (real solution)	γ_i
	[C$_4$mim][Tos] (1) + H_2O (2)	
0.960	343.3	0.991
0.860	333.2	0.927
0.754	324.0	0.870
0.707	318.9	0.834
0.629	310.7	0.793
0.592	305.7	0.762
0.523	296.7	0.726
0.501	292.2	0.696
0.477	285.8	0.650
0.442	280.0	0.631
0.408	272.2	0.599
	[C$_4$mim][Tos] (1) + Caprolactam (2)	
0.960	343.3	1.033
0.824	334.7	0.999
0.684	326.7	1.014
0.568	317.7	1.013
0.537	315.7	1.027
0.482	311.7	1.056
0.392	313.0	1.019
0.351	316.2	1.005
0.286	322.2	1.007
0.227	327.0	1.006
0.171	331.7	1.012
0.114	335.9	1.014
0.063	339.2	1.013

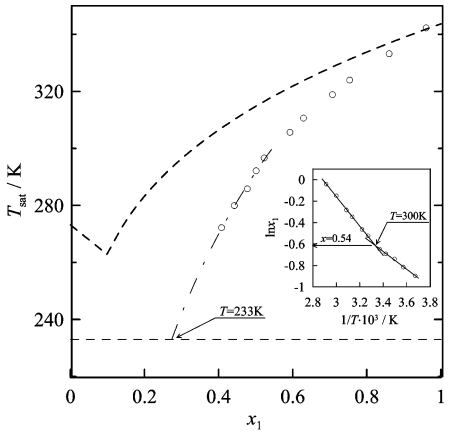

Figure 5. SLE diagram of the mutual solubility of [C$_4$mim][Tos] (1) + water: ○, experiment; --, ideal solution; - • -, extrapolation to the eutectic point.

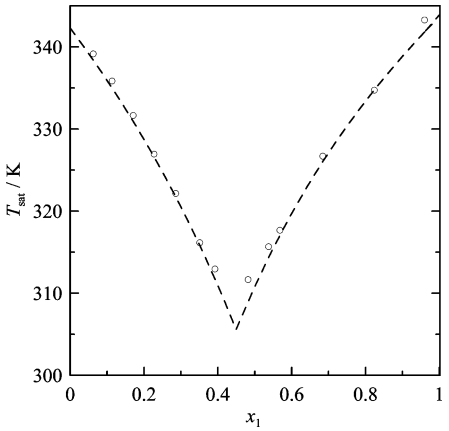

Figure 6. SLE diagram of the mutual solubility of [C$_4$mim][Tos] (1) + caprolactam: ○, experimental; - - -, ideal solution.

to the mole fraction of eutectic equal to 0.25 of [C_4mim][Tos] and 0.75 of H_2O.

(c) Heat Capacity of Sample No. 4: [C_4mim][Tos] (1)/H_2O (2), $x_1 = 0.30$. The experimental heat capacities of this sample are presented in Figure 3C and Table 3S (Supporting Information). The only important deviation in thermal behavior of sample no. 4 compared to sample no. 3 is the magnitude of the peaks. Their enthalpies are $\Delta_{trs}H°$ (233 K) = 19.5 J·g^{-1} and $\Delta_{fus}H°$ (300 K) = 34.5 J·g^{-1}.

For the sample containing $x_2 = 0.17$ of water in [C_4mim][Tos], two peaks at (342 ± 1) K and (300 ± 1) K were observed. For the samples containing $x_2 = 0.63$ and $x_2 = 0.70$ of water, the peak at $T = 342$ K was not presented, but the fusion peak at $T = 300$ K appeared. Its enthalpy amounted to $\Delta_{fus}H° = 44.8$ J·g^{-1} for sample no. 4. These data together with the SLE diagram (Figure 5) are consistent with the following conclusion. The [C_4mim][Tos]·$n$$H_2O$ crystalline hydrate melts at $T = (300 \pm 1)$ K with decomposition. The peak at $T = 342$ K corresponds to melting of pure [C_4mim][Tos]. Unfortunately, the data obtained here are not enough to calculate exactly the composition of the crystalline hydrate and the hydration enthalpy of [C_4mim][Tos]. These quantities were estimated based on the following assumptions: (1) $\Delta_{fus}H°_{[C4mim][Tos]}$ does not depend on the mole fraction of water in a sample; (2) the [C_4mim][Tos]·$n$$H_2O$ crystallohydrate fuses with decomposition; (3) the composition of eutectic is $x_2 = 0.75$ of water and $x_1 = 0.25$ of [C_4mim][Tos]; (4) the [C_4mim][Tos] mole fraction in crystalline hydrate exceeds 0.54 (footnote, Figure 5). The composition of the crystalline hydrate was found to be [C_4mim][Tos]·(0.7 ± 0.2)H_2O, and the hydration enthalpy was $\Delta_{hyd}H° = 7.1$ kJ·mol^{-1}. In other words, the process of decomposition of the crystalline hydrate is exothermic. To get more detailed information, the detailed study of the crystalline hydrate structure and the solution is required.

Conclusions

The heat capacity of [C_4mim][Tos] in the temperature range (5 to 370) K was measured by adiabatic calorimetry. It was found that depending on conditions of crystallization of a sample, [C_4mim][Tos] forms two crystalline modifications: cr I′ and cr I. Sigmoid anomalies in the heat capacity curves are related with formation of amorphous phases. The presence of the anomaly in a range of (280 to 300) K is caused by fusion of the [C_4mim][Tos]·$n$$H_2O$ hydrate.

Study of the phase equilibrium of [C_4mim][Tos] with water and caprolactam showed an essential difference in the nature of the formed solutions: the ([C_4mim][Tos] + caprolactam) solution is close to the ideal one whereas the ([C_4mim][Tos] + water) solution deviates from ideality even at low water content. The observed peritectic point in the SLE diagram for ([C_4mim][Tos] + water) corresponds to formation of crystallohydrate [C_4mim][Tos]·0.7H_2O that is in good agreement with the results obtained by adiabatic calorimetry. The eutectic of the [C_4mim][Tos]·$n$$H_2O$ crystalline hydrate was found at a ratio of [C_4mim][Tos]:H_2O = 1:3 and $T_e = (233 \pm 1)$ K.

Acknowledgment

The authors are grateful to Prof. A. Heintz from the University of Rostock (Germany) for providing the sample of ionic liquid.

Supporting Information Available:

Experimental heat capacity for mixtures of [C_4mim][Tos] with water. This information is available free of charge via the Internet at http: //pubs.acs.org.

Literature Cited

(1) Wilkes, J. S. Properties of ionic liquid solvent for catalysis. *J. Mol. Catal.* **2004**, *214*, 11−17.
(2) Fadeev, A. G.; Meagher, M. M. Opportunities for ionic liquids in recovery of biofuels. *Chem. Commun.* **2001**, 295−296.
(3) Holbrey, J. D. Industrial applications of ionic liquids. *Green Chem.* **2005**, *7*, 35−37.
(4) Shimizu, Yo.; Ohte, Yo.; Yamamura, Ya.; Saito, K.; Atake, To. Low-temperature heat capacity of room-temperature ionic liquid, 1-hexyl-3-methylimidazolium bsi(trifluoromethylsulfonyl)imide. *J. Phys. Chem.* **2006**, *110*, 13970−13975.
(5) Paulechka, Y. U.; Kabo, G. J.; Shaplov, A. S.; Lozinskaya, E. I.; Vygodskii, Ya. S. Thermodynamic properties of 1-alkyl-3-metylimidazolium bromide ionic liquids. *J. Chem. Thermodyn.* **2007**, *39*, 158−166.
(6) Kabo, G. J.; Blokhin, A. V.; Paulechka, Y. U.; Kabo, A. G.; Shymanovich, M. P.; Mage, J. W. Thermodynamic Properties of 1-Butyl-3-methylimidazolium Hexafluorophosphate in the Condensed State. *J. Chem. Eng. Data* **2004**, *49*, 453−461.
(7) Blokhin, A. V.; Kabo, G. J.; Paulechka, Y. U. Thermodynamic properties of [C_6mim][NTf_2] in the condensed state. *J. Chem. Eng. Data* **2006**, *51*, 1377−1388.
(8) Paulechka, Y. U.; Kabo, G. J.; Blokhin, A. V.; Vydrov, O. A.; Magee, J. W.; Frenkel, M. Thermodynamic Properties of 1-Butyl-3-methylimidazolium Hexafluorophosphate in the Ideal Gas State. *J. Chem. Eng. Data* **2003**, *48*, 457−462.
(9) Zaitsau, Dz. H.; Kabo, G. J.; Strechan, A. A.; Paulechka, Y. U.; Tschersich, A.; Verevkin, S. P.; Heintz, A. Experimental vapor pressures of 1-alkyl-3-methylimidazolium-bis-(trifluoromethanesulfonyl) imides and a correlation scheme for estimation of vaporization enthalpies of ionic liquids. *J. Phys. Chem. A* **2006**, *110*, 7303−7306.
(10) Rossini, F. D.; Pitzer, K. S.; Arnett, R. L.; Braun, R. M.; Pimentel, G. C. *Selected values of physical and thermodynamic properties of hydrocarbons and related compounds*; Carnegie Press: Pittsburgh, 1953.
(11) Kabo, A. G.; Blokhin, A. V. Scanning calorimeter for the heat capacity measurements in a temperature range from 270 to 700 K. XV Russian International Conference on Chemical Thermodynamics. Book of abstract **2005**, *1*, 123.

Received for review March 25, 2007. Accepted June 17, 2007. The work was supported by the INTAS-Belarus grant No. 03-50-5526.

JE700152C